On the Annual Cycle of Latent Heat Fluxes over

the Equatorial Pacific Using TAO Buoy Observations

By Hae-Kyung Lee, Pao-Shin Chu

Department of Meteorology, School of Ocean and Earth Science and Technology,
University of Hawaii, Honolulu, Hawaii, U.S.A.

C.-H. Sui and K.-M. Lau

Climate and Radiation Branch, Laboratory for Atmospheres, NASA/Goddard Space Flight Center,
Greenbelt, MD, U.S.A.

Abstract

In this paper, we describe the annual cycle in the latent heat flux (LHF) and its associated bulk variables (sea surface temperature, wind speed, humidity difference) over the equatorial Pacific. The in-situ, daily-averaged TAO buoy observations between 8°N and 8°S during the period 1992–1996 form the database. LHF was computed using a modified bulk parameterization scheme to account for active convection and low wind speed frequently observed in the western Pacific. Harmonic analysis was used to help quantify the phase and amplitude of the annual and semiannual cycles.

The annual cycle of LHF was found to be conspicuous in two regions, namely, the northeastern and western/central Pacific. For the former region, the maximum LHF occurs in boreal summer and early fall, when surface wind speeds are strong and the temperature difference between sea surface and air near the bottom of the atmospheric boundary layer is large. For the western/central Pacific, maximum LHF occurs in boreal winter, when the winter monsoon is strong. In contrast to the aforementioned two regions, the annual cycle in LHF in the equatorial cold tongue is weak and low LHF prevails throughout the year. Also noted in this study is a westward propagation of the maximum LHF region from the northeastern Pacific around July to the western Pacific by the following March.

We also ascertained the relative importance of dynamic and thermodynamic processes in regulating the month-to-month variations of the LHF along two meridional transects, one in the eastern and another in the western Pacific. In the eastern Pacific, except to the north of the cold tongue, variations in humidity difference (*i.e.*, thermodynamic process) seem to be of primary importance to the annual variations in LHF. On the other hand, variations in wind speed (*i.e.*, dynamic process) are more important to the LHF in the western/central Pacific.

1. Introduction

Latent heat flux is one of the most important components in the surface heat budget over the tropical oceans. It is also a major source of atmospheric energy, particularly for thunderstorms and hurricanes. Latent heat flux, together with sensible heat and momentum fluxes, determines the major part of ocean and atmosphere interaction, and thus climate variability.

Corresponding author: Pao-Shin Chu, Department of Meteorology, School of Ocean and Earth Science and Technology, University of Hawaii, 2525, Correa Road, Hawai'I 96822-2219, Honolulu, Hawaii 96822, U.S.A.

In the past, there have been many efforts to estimate sensible and latent heat fluxes over the tropical Pacific (*e.g.*, Weare *et al.*, 1981; Esbensen and Reynolds, 1981; Esbensen and Kushnir, 1981; Reed, 1985; Oberhuber, 1988; Liu, 1988; Chou *et al.*, 1995; da Silva *et al.*, 1995). With the exception of Liu (1988) and Chou *et al.* (1995), long-term ship records and marine weather reports are generally used in research communities to obtain surface heat fluxes for climate studies. These studies provided useful information regarding spatial and temporal variability of fluxes.

However, accurate flux cannot be ascertained from these climatic records because of the

observation- and instrumentation errors inherent in data from the non-research ships. For example, differences in instrumentation and in heights of anemometers among different types of ships may cause a large discrepancy in ship-reported wind velocities. Furthermore, ship observations are confined along the narrow ship tracks, leaving a large portion of the oceans with little or no data (Sadler et al., 1987). Satellite data may cover more area than ship data, but retrieved near-surface meteorological parameters also contain large uncertainties.

Recently, Zhang and McPhaden (1995, hereafter referred to as ZM) studied the relationship between latent heat flux and sea surface temperature (SST) over the equatorial Pacific Ocean based on the two-year (1991–93) research-quality Tropical Atmosphere Ocean (TAO) moorings. Unlike ship data, instrumental errors in TAO data are small. ZM chose three buoys that represent the western, central, and eastern Pacific, and they showed a pronounced annual cycle in the latent heat flux (hereafter referred to as LHF) over the western Pacific but less so over the eastern Pacific. Esbensen and McPhaden (1996) also used TAO moored buoy records to study tropical ocean evaporation. They noted that uncertainties of surface evaporation based on daily mean data are usually 10 % or less than the total moisture flux.

There are now about five years of TAO records (1992–96) available for analysis. It is thus meaningful to determine the spatial distribution as well as the temporal variability of the LHF over the entire equatorial Pacific, with the objective to document the annual cycle of LHF using the research-quality TAO data. We will also shed light on the mechanisms responsible for the annual variations of LHF. In Section 2, we describe the data, bulk algorithms, and the harmonic method used, and in Section 3 the annual cycle of the bulk variables and LHF in the equatorial Pacific based on the records averaged from 1992 to 1996. In Section 4, we detail the result of the harmonic analysis; in Section 5, we focus on the relative importance of dynamic and thermodynamic processes in regulating heat fluxes along two meridional transects representative for the eastern and western Pacific. Section 6 contains the summary and conclusion.

2. Data and methodologies

2.1 Data

In this study, daily-averaged TAO buoy data (wind, air temperature, relative humidity, and sea surface temperature) from the NOAA's Pacific Marine Environmental Laboratory are used. Sea surface temperature and wind speed are measured at 1 m depth and 3.8 m above the ocean surface, respectively. The nominal observation height for air temperature and relative humidity is 3 m. Daily wind speeds from TAO are computed as vector averages

from hourly observations (ZM). We use 64 moorings deployed in the equatorial Pacific basin, spanning a region approximately 8°N–8°S, 95°W–137°E (Fig. 1a).

The TAO measurements began in the middle 1980s and relative humidity sensors were added to the moorings in 1989 (McPhaden, 1993). However, a majority of buoys did not have humidity sensors until 1992. Accordingly, we will use all the TAO buoys over the period from 1992 to 1996 for studying the annual variations of the LHF over the entire equatorial Pacific. Fig. 1b shows the spatial distribution of the total number of days with TAO records from 1992 to 1996. Clearly, observations are plentiful in the central portion of the basin. Fewer records are found in the extreme western Pacific, implying less reliable results in this area.

2.2 Bulk parameterization scheme

Surface latent heat fluxes are computed based on a bulk parameterization scheme similar to Liu et al. (1979, hereafter referred to as LKB) with some modifications suggested by Fairall et al. (1996). A brief description follows. The surface moisture fluxes (E) are defined as

$$E = L_v \rho C_E U (q_s - q) \tag{1}$$

where L_v is the latent heat for evaporation and ρ the density of air. Here, C_E denotes the turbulent exchange coefficient for water vapor and U is wind speed at a reference height. Water vapor mixing ratio at a reference height and saturation water vapor mixing ratio at the SST are represented by q and q_s, respectively.

Moisture in the atmospheric surface layer is assumed to take the following forms:

$$q(z) - q_s = q_*/k \left[\ln(z/z_q) - \psi_q\right] \tag{2}$$

where k is the von Karman constant (0.4), and q_* is the scaling moisture; z is the height where the TAO sensor measurements are made (3 to 4 m); and z_q is moisture roughness length. In (2), ψ_q is a stability function for moisture that depends on z/L, where L is the Monin-Obukhov length expressed as a function of frictional velocity (u_*), virtual temperature (T_v), and equivalent virtual temperature (T_v^*).

z_q is obtained following LKB. Specifically,

$$z_q = \nu c R r^d / u_* \tag{3}$$

where Rr is the roughness Reynolds number, ν is the kinematic viscosity, and c, d are functions of Rr given in LKB.

According to the bulk formulas, the LHF (E) depends on the wind speed, turbulent transfer coefficient for water vapor, and the humidity difference between the SST (T_s) depth and the air above the sea surface. In regions where wind speeds are low (say around 0.5 m s^{-1}), the LKB scheme may break

Fig. 1. Fig. 1. (a) Locations of the TOGA-TAO buoys. The equatorial cold tongue, following Bjerknes
(1969) definition, is enclosed by a thin solid line. (b) Total number of days with TAO buoy observa-
tions from 1992 to 1996.

down (Godfrey and Beljaars, 1991) and needs to be modified. Therefore, the original LKB scheme has been modified to include a gustiness factor. The gustiness velocity is defined as

$$W_g = \beta(-u_* b_* z_i)^{1/3} \qquad (4)$$

where $\beta = 1.25$, $b_* = gT_v^*/T_v$, and $z_i = 600$ m. Since the gustiness factor is added to the measured wind speed, which is expressed as $(u^2 + v^2 + W_g^2)^{1/2}$, the wind used here is therefore prevented from being underestimated in light wind conditions. Fluxes computed by the present algorithm using TOGA COARE observations were reported in Sui et al. (1997) and were found to be in close agreement with that based on the COARE scheme (Fairall et al., 1996).

2.3 Effects of cool-skin temperature and warm layer

It would be more accurate to estimate LHF at the ocean-atmosphere interface using the ocean skin temperature, instead of relying on temperature at 1-m depth as in this study. This interface is cooler than the water below (the so-called cool skin effect). The solar radiation, on the other hand, warms the surface temperature and this warm layer may be less than one meter deep (the so-called warm layer effect).

Fairall et al. (1996) modified the LKB parameterization scheme by taking the cool skin and warm

layer effects into account using data from TOGA COARE. However, since the Fairall et al. algorithm (COARE algorithm) requires shortwave and longwave radiation as input, which are not available from buoy observations used in this study (1992–96), it is not possible to determine the ocean skin temperature from buoy observations. It is interesting to note that Zhang (1995) compared the monthly mean latent heat fluxes computed from the COARE algorithm and the algorithm which does not include the effects of warm layer and cool skin. Using prescribed values for solar radiation and downward longwave radiation, Zhang (1995) showed that the monthly mean latent heat fluxes for a buoy at 0°, 156°E from the aforementioned two algorithms are in good agreement (within a few watts per square meter). More recently, based on the entire array of TAO buoys, Zeng and Dickinson (1998) also reached the same conclusion. We thus feel that the bulk scheme with the use of SST at 1-m depth in this study may also yield reasonable estimates of latent heat fluxes, particularly on the climate time scale.

3. The annual cycle in bulk parameters and heat flux

For this work, three bulk parameters (SST, wind speed, and humidity difference), the associated LHF, and the difference between SST and air tem-
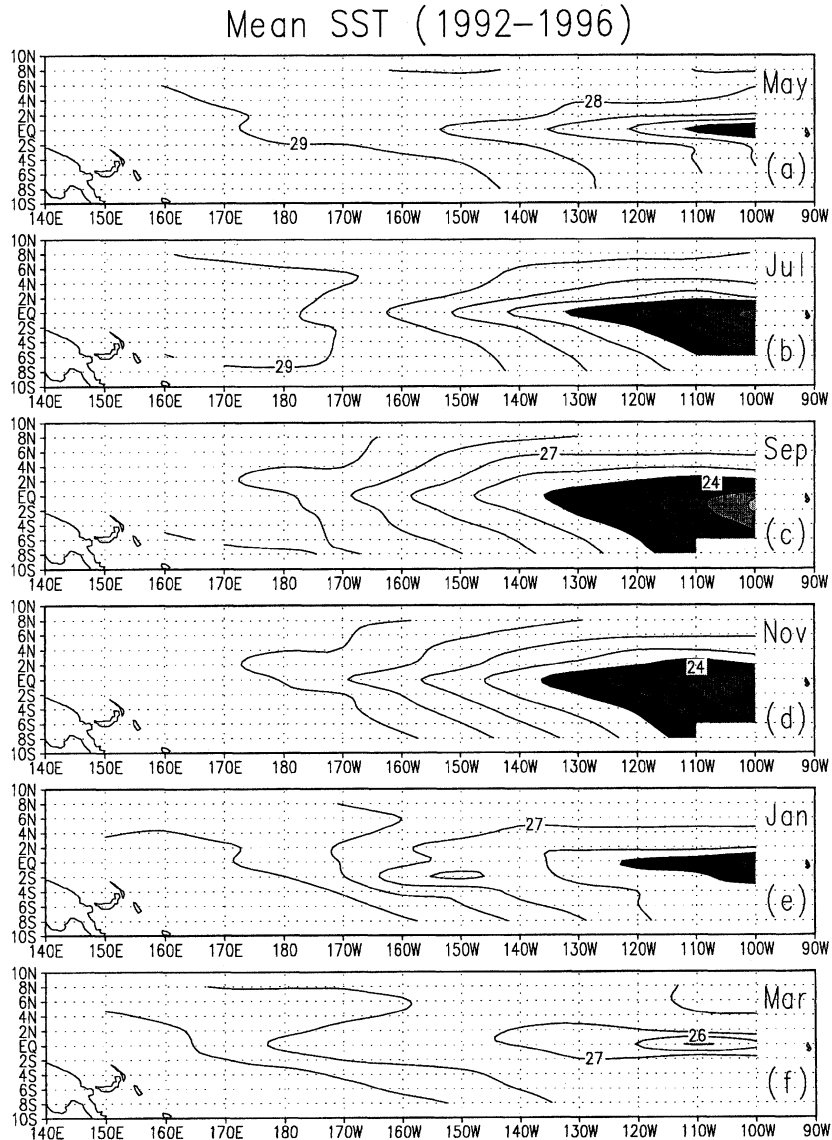
Mean SST (1992–1996)

Fig. 2. Monthly mean sea surface temperature (K) based on TAO buoys during 1992–96 over the tropical Pacific. (a) May, (b) July, (c)September, (d) November, (e) January, and (f) March. Contour interval is 1 K. Shading indicates SST less than 25°C.

perature are presented for every other month. To facilitate the discussion, we begin in May. The 5-yr (1992–96) climatological monthly mean flux is calculated from the daily mean flux. Because of the prolonged warming in the tropical Pacific during 1991 and 1995 (Trenberth and Hoar, 1996), LHF presented in this study may be biased toward the warm event and thus should not be viewed as representing long-term climatological conditions.

The annual cycle of SST in the tropical Pacific has been the subject of many studies (e.g., Horel, 1982; Mitchell and Wallace, 1992; Koberle and Philander, 1994; Wang, 1994; Xie, 1994). Xie (1994) suggested that the driving mechanisms of SST on the El Niño Southern Oscillation (ENSO) and the annual cycle timescales are different. On the ENSO time scale,

the change in the thermocline depth is the major factor for SST variations. However, on the annual cycle time scale, vertical mixing in the upper ocean becomes the primary cause of SST variations; this is particularly clear in the eastern Pacific, where there is a little change in the thermocline depth on this timescale.

Figure 2 shows the spatial distributions of monthly mean SST. In May (Fig. 2a), the warm sea surface water (> 29°C) in the western Pacific and the narrow cold tongue axis along the equator from 100°W to 150°W are conspicuous. With the approach of austral winter (July), the enhanced southeasterlies (Fig. 4b) may increase the vertical mixing in the upper ocean. This mechanism causes SSTs in the eastern equatorial Pacific to drop appre-

Mean Latent Heat Flux (1992-1996)
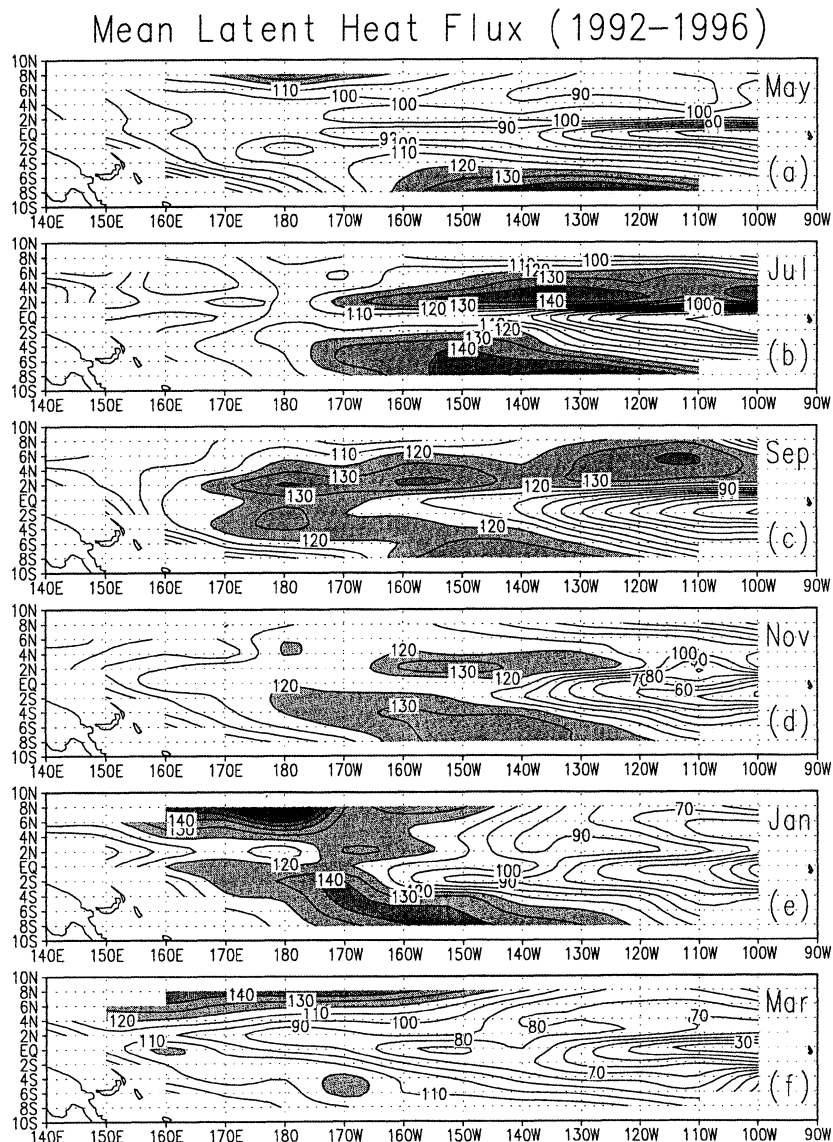
Fig. 3. Same as Fig. 2, except for latent heat flux in W m^{-2}. Contour interval is 10 W m^{-2}. Shading indicates LHF greater than 120 W m^{-2}.

ciably from May to July (Figs. 2a and 2b). Consequently, the axis of the cold tongue extends farther westward to 160°W. By September (Fig. 2c), the cold tongue is fully developed with its axis expanding westward to about 165°W and this pattern remains until November (Fig. 2d). Note that the maximum cooling in September occurs at the easternmost boundary ($\sim$ 100°W) where the thermocline is shallowest (Myers, 1979). A slack zonal SST gradient and gradual warming occurs in the equatorial eastern Pacific during January and March (Figs. 2e and 2f). SST variations in the western Pacific warm pool region are comparatively small from one season to another.

Figure 3a shows the distribution of the mean latent heat flux for May. Relatively low values of LHF prevail in the bulk of the Pacific with a minimum

value along the equator extending from 100°W westward to about 174°W. Large values ($\geq$ 120 W/m^{**2}) are found mainly in the South Pacific poleward of 6°S extending from about 160°W to 110°W. In July, the salient features include the continued development of high LHF in the South Pacific and the formation of an extensive, new, zonally oriented band of high LHF in the northeastern Pacific from 170°W to 100°W (Fig. 3b). As previously shown, the cold tongue expands and possibly deepens from May to July (Figs. 2a and 2b). The southeasterly tradewinds in the south Pacific, once across the cold tongue, would advect cold air northward over the relatively warm ocean surface to form an unstable atmospheric boundary layer. This unstable vertical stratification over the northeastern Pacific may enhance downward transport of momentum fluxes,

Mean Wind Speed and Vector (1992–1996)
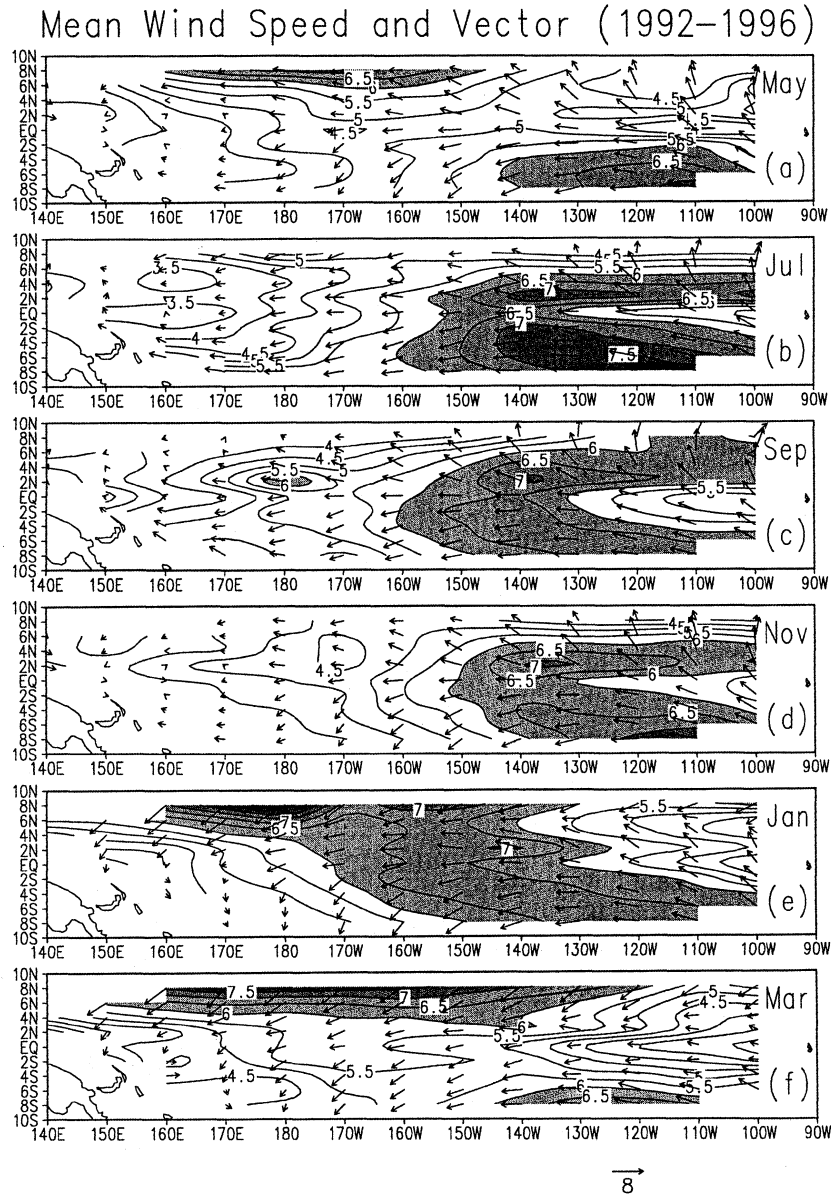
Fig. 4. Same as Fig. 2, except for wind speed in m s^{-1}. Contour interval is 0.5 m s^{-1}. Shading indicates wind speed greater than 6 m s^{-1}.

increasing the wind speed near the surface (Figs. 4a and 4b; Wallace *et al.*, 1989; Deser and Wallace, 1990). As a result, there is a substantial increase in LHF in the northeastern Pacific in July (Fig. 3b).

As a crude measure of stability condition in the atmospheric boundary layer, Figure 5 shows the spatial distribution of the difference between SST and air temperature at 3 m above the ocean surface. A positive difference is noted in the entire equatorial Pacific throughout the year. However, this difference is larger ($\geq$ 1°C) in the northeast Pacific from May to November (Figs. 5a to 5d), implying a more unstable condition near the bottom of the atmospheric boundary layer when strong southeast trades cross the equatorial cold tongue.

The humidity difference between the tropical at-

mosphere and ocean in the western Pacific exhibits a distinct seasonality (Fig. 6). This is readily seen as an increase in the area of high dq ($>$ 6 g/kg) in the western Pacific from May to November. The area of high dq in the western Pacific diminishes pronouncedly from November to March, and the area of high dq in boreal winter is mainly confined to the southwest Pacific. In contrast to the western Pacific, dq in the eastern Pacific is relatively low and changes are insignificant from one season to another.

Returning to Fig. 3b, the two bands of the high LHF, one in each hemisphere, continue to extend farther west by September (Fig. 3c) and then merge with each other in the equatorial central-western Pacific (170°W to 170°E) where this increase in LHF coincides with an enhancement of dq (Fig. 6c) and
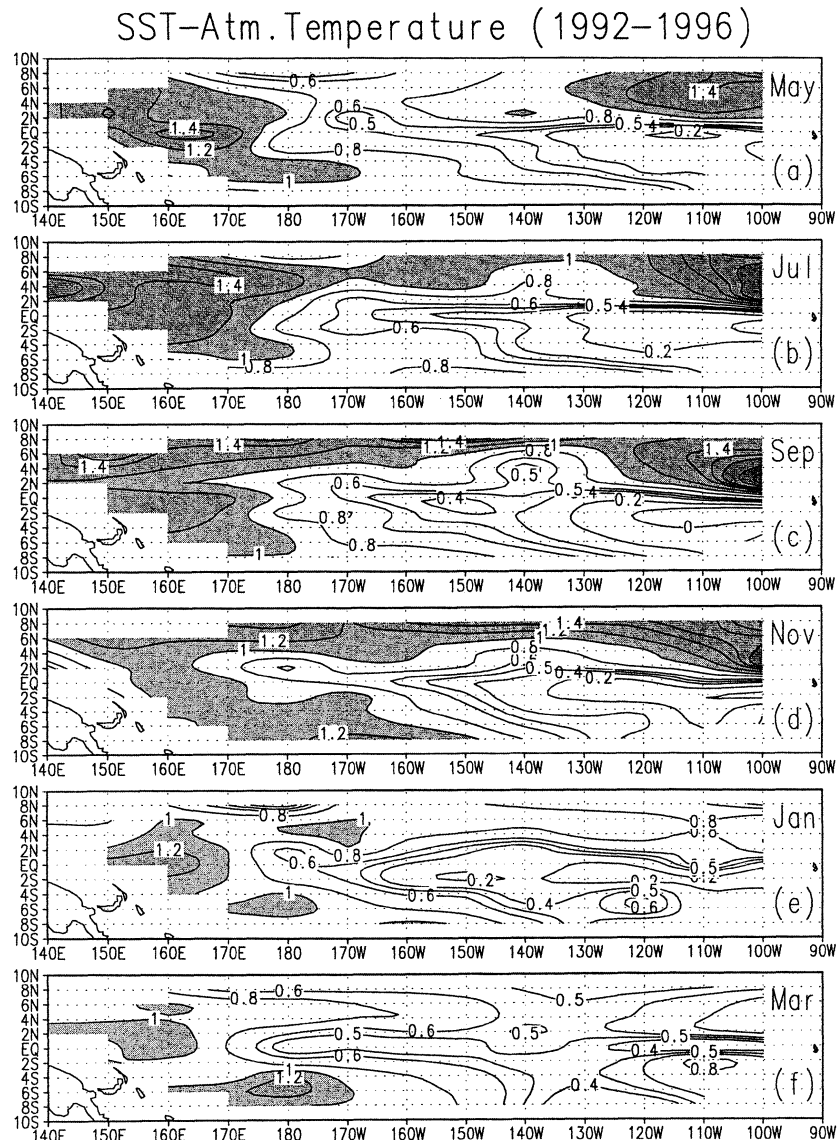
Fig. 5. Same as Fig. 2, except for difference between SST and air temperature (°C). Shading indicates temperature difference greater than 1°C.

wind speed (Fig. 4c). Low LHF occurs in the cold tongue region where dq is low (Figs. 3c, and 6c).

By November (Fig. 3d), the two bands of high LHF, one in each hemisphere, are still discernible in the central Pacific. The arrival of the East Asian/western Pacific winter monsoon, and the accompanying northeasterly surges enhance surface wind speeds in the northwest Pacific in January (Fig. 4e); this gives rise to an increase in LHF in the northwestern and central Pacific (Fig. 3e). In the meantime, minimum LHF still resides over the eastern Pacific. As the eastern Pacific gradually warms up from January to March (Figs. 2e and 2f), wind speed decreases over much of the equatorial Pacific in March (Fig. 4f). Consequently, most of the equatorial Pacific is characterized by a low LHF in March (Fig. 3f).

4. Harmonic analysis of latent heat flux and bulk parameters

Harmonic analysis has commonly been used to determine the annual fluctuations of a geophysical time series. Horel (1982), among others, used harmonic analysis to demonstrate the geographic distributions of annual cycles of major meteorological variables. To simplify working with a large number of figures, a harmonic dial was used so that the amplitude and phase of the annual variation in different geographic regions could be compactly presented in a single figure. We will use the harmonic dial to illustrate the annual cycle of fluxes over the equatorial Pacific. The annual cycle refers to the first harmonic of the annual variation. See Appendix for details on harmonic analysis.

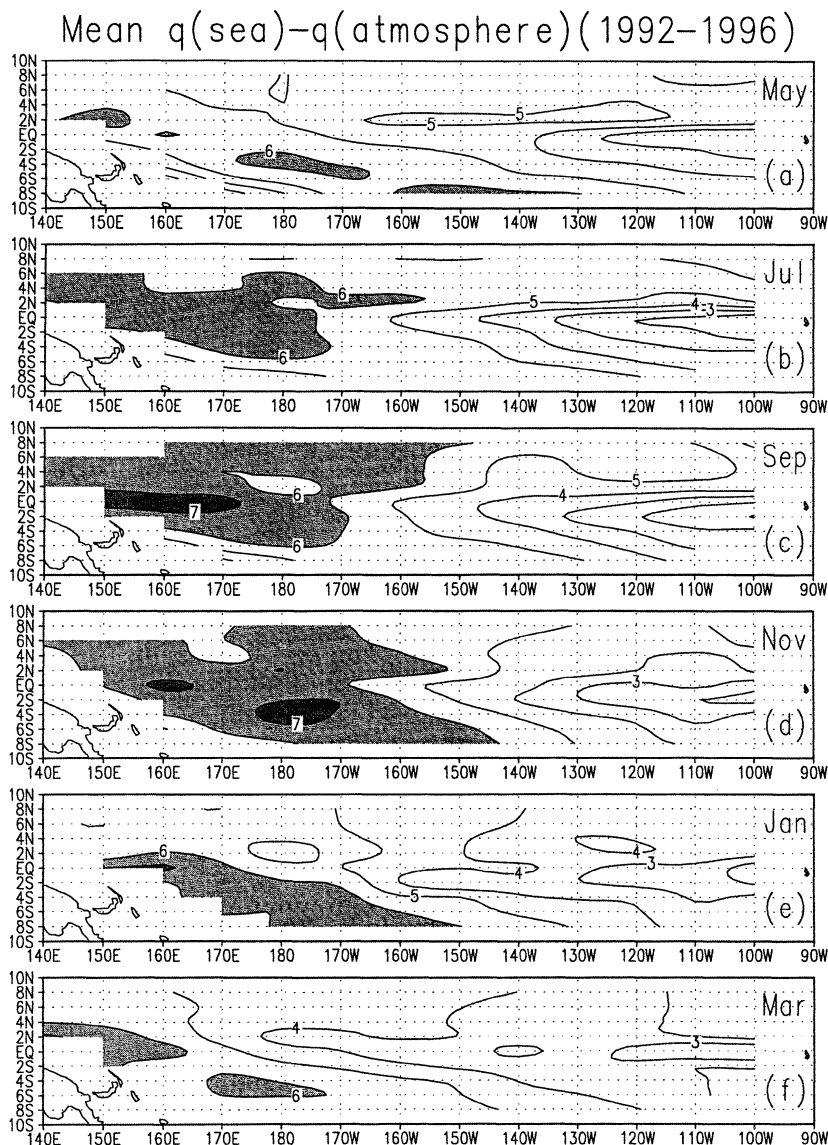Figure 7 shows the first harmonic dial of the an-

Mean q(sea)-q(atmosphere)(1992-1996)

Fig. 6. Same as Fig. 2, except for humidity difference in g kg^{-1}. Contour interval is 1 g kg^{-1}. Shading indicates dq greater than 6 g kg^{-1}.

nual cycle of the SST, LHF, wind speed, and humidity difference in the equatorial Pacific, respectively. For SST (Fig. 7a), the large amplitude of the annual cycle is found in the equatorial cold tongue region, and this amplitude diminishes noticeably from the eastern to the central Pacific ($\sim 155°$W). The annual cycle in SST in the cold tongue region also undergoes systematic longitudinal changes in phase. For example, the warmest surface water occurs in April near 95°W and progressively later in the year (July) as the central Pacific ($\sim 155°$W) is approached. The annual cycle in SST in the cold tongue region also appears to lead the corresponding phase of SST in an area to the north of the cold tongue by about one to two months. Accordingly, the highest SST to the east of 140°W in the northeast Pacific is observed around June.

In Fig. 7b, the most notable features are the large amplitudes and the rather systematic changes in phase of the annual cycle of the LHF across a large, elongated area from the northeast Pacific extending westward to the dateline. Specifically, along 5°N, the maximum of flux at the longitude of 110°W occurs near August, at 140°W in September, at 155°W in October and near the dateline in December. A relatively weak annual cycle exists over much of the cold tongue region. In a broad sense, the phase of the maximum LHF in the northeastern and central Pacific lags behind the corresponding phase of the maximum dq (Fig. 7d) by about one month, implying that maximum dq in these regions is related to the maximum LH throughout the year. The maximum of the wind speed in the aforementioned regions tends to occur about one month later than the
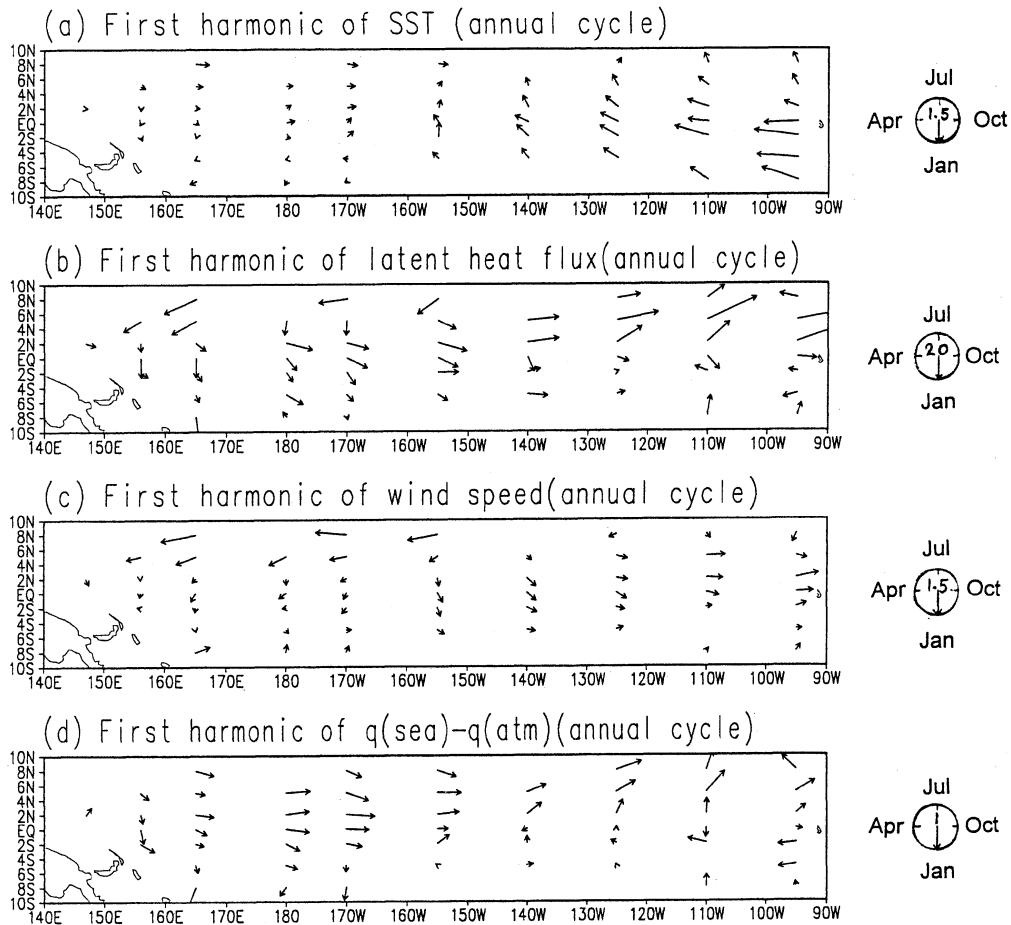
Fig. 7. Harmonic dials depicting phase and amplitude of the first harmonic (annual cycle) of (a) SST, (b)latent heat flux, (c) wind speed, and (d)humidity difference. The amplitude of the annual cycle is indicated by the length of the arrow according to the scale in the figure. Scales of the amplitude of latent heat flux, wind speed, and humidity difference are 20 W m^{-2}, 1.5 m s^{-1}, and 1 g kg^{-1}, respectively (see clock displayed on the right of each panel). The phase is indicated by the direction of the arrow. An arrowhead pointing from the top of the page indicates a maximum on 1 January.

corresponding maximum in LHF (Figs. 7b and 7c).

In the northwest Pacific (west of the dateline), the phase of the annual cycle in LHF is distinctly different from that in the east and south (Fig. 7b); the phase of the maximum wind speed in the annual cycle (Fig. 7c) appears to coincide approximately with the corresponding phase of the heat flux (Fig. 7b), with a maximum value occurring in March. Hence, the annual cycle of LHF in the northwestern Pacific appears to be intimately governed by wind speeds.

Figure 8 illustrates the meridionally averaged LHF (8°N–8°S) in a time-longitude cross section. A westward propagation of the maximum in latent heat flux is seen, starting from about 140°W in July to about 150°E in the following March. It should be noted that the sample size may become too small if the meridional average is taken only for each hemisphere. For instance, only two buoys are available along 140°W in the North Pacific. Therefore, the meridionally averaged values from the entire longi-

tudinal domain from 8°N to 8°S are used.

The westward phase propagation of the maximum LHF seems to be related to the westward expansion of the cold tongue during boreal fall (Fig. 2). When the cold tongue is best developed (September), the area to the north of the cold tongue (say somewhere north of 2°N) experiences cold advection aloft, which then enhances the surface wind speed and humidity difference through vertical transport of momentum fluxes (Deser and Wallace, 1990). The increase in bulk parameters naturally leads to an increase in LHF and accounts for a maximum in LHF immediately to the north of the cold tongue in September (Fig. 3c). Since SST in the cold tongue exhibits a strong annual cycle (Figs. 2 and 7a), the annual cycle of LHF is also strong in the area north to the cold tongue.

It is also instructive to examine the proportion of variance explained by the leading harmonics. Figure 9a shows that the variance accounted for by the
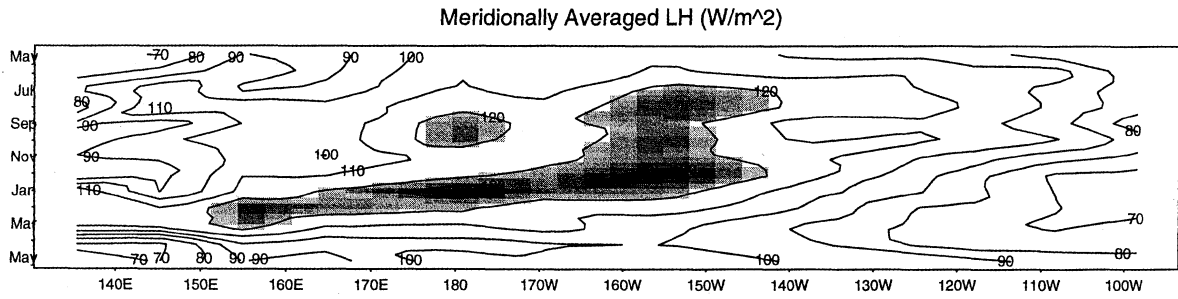
Meridionally Averaged LH (W/m^2)

Fig. 8. Time-longitude cross section of the meridionally averaged latent heat flux between 8°N and 8°S over the equatorial Pacific basin. Shading denotes values greater than 120 W m^{-2}.
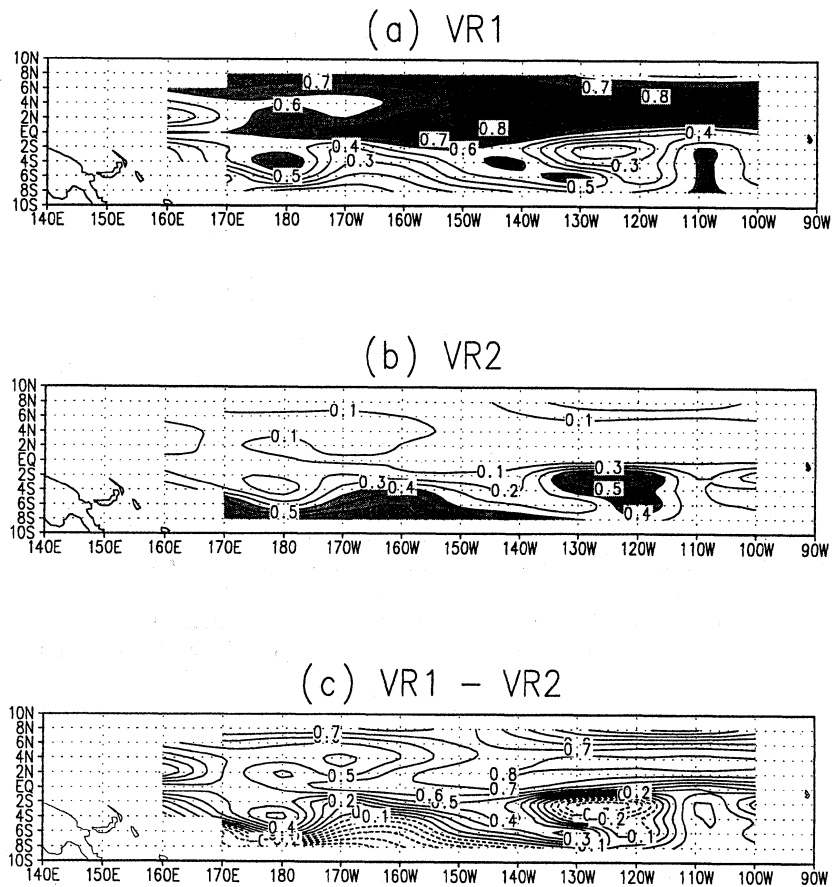
(a) VR1

(b) VR2

(c) VR1 − VR2

Fig. 9. Contour plot of (a) the fractional variance of the first harmonic (annual cycle) of latent heat flux, (b) the fracional variance of the second harmonic (semiannual cycle) of latent heat flux, and (c) the difference in fractional variance between the first and second harmonic. Shading in (a) indicates regions with fractional variance exceeding 60 % and in (b) indicates regions with fractional variance exceeding 40 %. Broken lines in (c) denote negative values.

first harmonic (VR1, hereafter) is large (more than 0.6) in the northeast and northwest Pacific. For the second harmonic (VR2, hereafter), a large area bounded between the equator and 8°S and 135°W and 115°W shows a relatively high percentage of the variance in LHF (Fig. 9b), with a particularly large value in the core of the cold tongue region. This is also supported by the time series plot of the LHF at

2°S, 125°W where a semiannual cycle is conspicuous (Fig. 10a). Interestingly, this pronounced semiannual cycle of LHF in the cold tongue is somewhat unexpected given the well-known strong annual cycle in the SST in this region (Figs. 2 and 7a). A large semiannual cycle is also found over the southwest Pacific (Figs. 9b and 9c, and 10b).
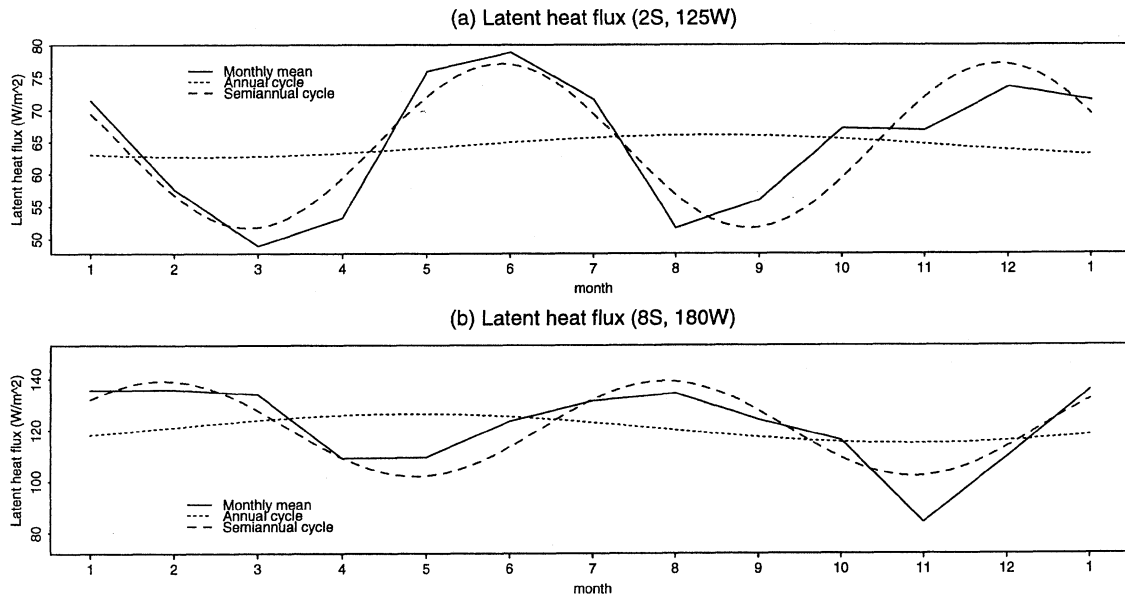
Fig. 10. Time series of the monthly mean LHF, the annual cycle, and the semiannual cycle of LHF for the equatorial cold tongue (a) and the southwest Pacific (b).

5. Relative importance of dynamic and thermodynamic processes in regulating LHF

In order to clarify the relative role of dynamic and thermodynamic processes in regulating the LHF, the monthly variation of LHF is partitioned into several components. Here, while keeping L_v, ρ and C_E unchanged, Eq. (1) may be rewritten as

$$E = L_v\rho C_E U dq = L_v\rho C_E(\overline{U} + U')(\overline{dq} + dq') \quad (5)$$

where the overbar denotes the annual mean and prime denotes deviation from the annual mean. The right hand side of (5) consists of four terms involving $\overline{U}\,\overline{dq}$, $\overline{U}dq'$, $U'\overline{dq}$, and $U'dq'$.

We select two meridional transects where data are more abundant for illustrating the relative contributions of the above terms to the total variations in E. Figure 11 shows the latitude-time cross section of the monthly variations of LHF along 110°W. The top panel refers to the total month-to-month variation of the LHF induced by both variations in wind speed and humidity difference, which is defined as the difference between the monthly mean LHF and the annual mean flux. For simplicity, this difference is referred to as the total variation.

In the eastern Pacific, a similar pattern is noted between the total variation of LHF (Fig. 11a) and the variation of LHF induced by changes in dq while holding wind speed constant (Fig. 11b). It is interesting to note that the increase of LHF from March to June in the southeast Pacific in Fig. 11a is associated with a corresponding increase in dq' (Fig. 11b). Starting in July, the sharp decrease in dq' (Fig. 11b) due to the rapid development of the cold tongue re-

sults in a decrease in the LHF along the equator (Fig. 11a). As southeasterlies intensify during boreal summer, LHF as induced by changes in wind speed increases in an area to the north of the cold tongue (Fig. 11c), and this increase is comparable to the variation of LHF induced by changes in dq (Fig. 11b). The monthly variations of LHF due to the covariance between wind speed and humidity difference are shown in Fig. 11d. In general, the values are less than 6 W m^{-2} most of the time. These results suggest the importance of the thermodynamic process in regulating the latent heat flux in the eastern Pacific. The exception is the region to the north of the cold tongue, where dynamic processes play an equally important role as thermodynamic processes in the variation of LHF.

In the western Pacific, a striking similarity is found between the total variation in LHF and the LHF induced by variations in wind speed (Figs. 12a and 12c) throughout the year, suggesting the dynamic processes as the important mechanism in regulating heat fluxes in the western Pacific. Also note positive values in LHF due to change in dq during boreal summer in the northwestern Pacific (Fig. 12b). However, these positive values are smaller than the corresponding negative values in LHF due to change in wind speed (Fig. 12c), thus resulting in a net large decrease in LHF during boreal summer in the northwestern Pacific, as seen in Fig. 12a. The variation of LHF due to the covariance between wind speed and humidity difference can sometimes be important, particularly in the north Pacific from July to October (Fig. 12d).
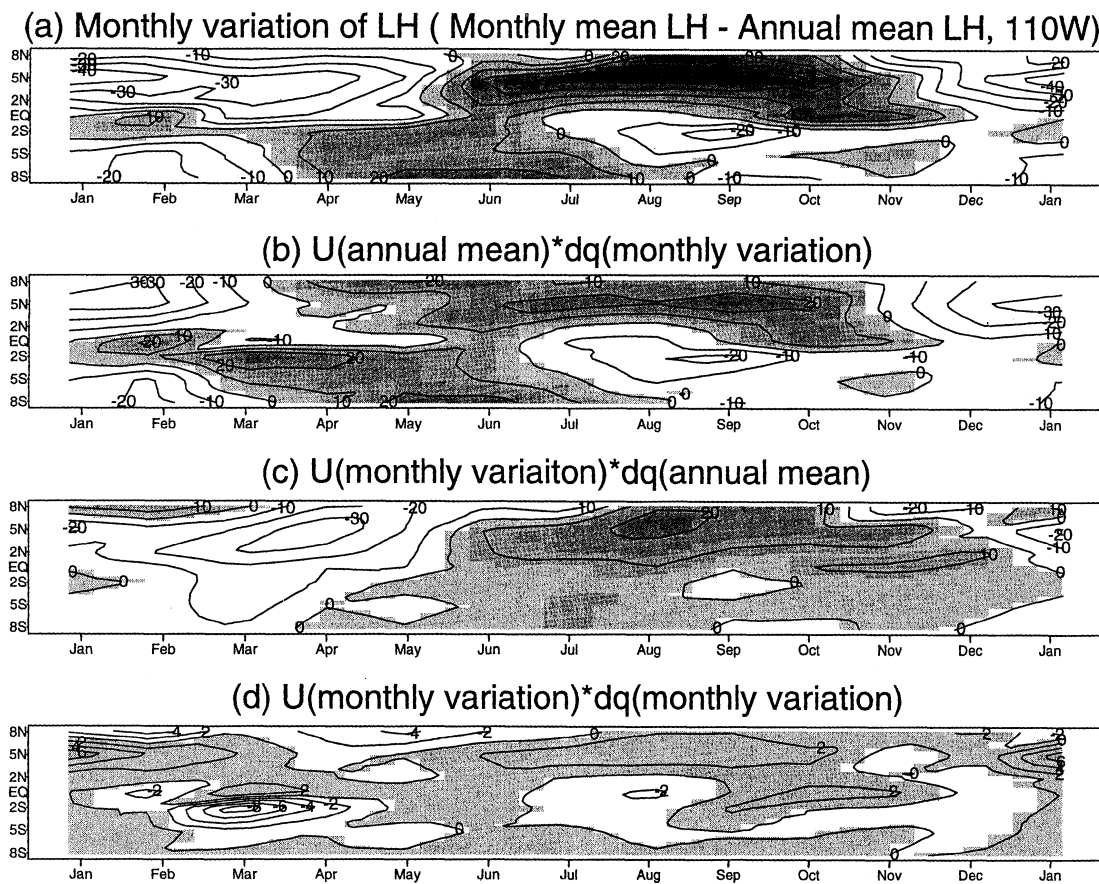
(a) Monthly variation of LH (Monthly mean LH - Annual mean LH, 110W)

(b) U(annual mean)*dq(monthly variation)

(c) U(monthly variaiton)*dq(annual mean)

(d) U(monthly variation)*dq(monthly variation)

Fig. 11. Time-latitude cross section of the total monthly variations of LHF (*i.e.*, $L_v \rho C_E (\overline{U} + U')$ $(d\overline{q} + dq') - L_v \rho C_E \overline{U} d\overline{q})$ along 110°W (a), monthly variations of LHF induced by dq (*i.e.*, $L_v \rho C_E \overline{U} dq'$) (b), monthly variations of LHF induced by wind speed (*i.e.*, $L_v \rho C_E U' d\overline{q}$) (c), and monthly variations of LHF due to covariance between wind speed and humidity difference (*i.e.*, $L_v \rho C_E U' dq'$) (d). Shading indicates positive values.

6. Summary and conclusions

In this study, the high quality in-situ TAO data and the improved bulk formulas are used to investigate the annual cycle of the moisture flux at the air-sea interface over the entire equatorial Pacific Ocean. The daily-averaged data from a large number of TAO moorings for the years 1992 to 1996 are used to obtain a five-year mean monthly flux.

Distinct annual cycles are identified in two regions: Northeast Pacific (north of the cold tongue) and central/western Pacific. For the former region, low LHF is found from January to March when the SST in the equatorial eastern Pacific is moderately warm, wind speed is weak and humidity difference is small. High LHF prevails from July to September when surface wind speeds are strong, the meridional SST gradient is large, and the vertical temperature difference between sea surface and the bottom of the atmospheric boundary layer is large. The vertical momentum transfer, as induced by cold air advection due to enhanced southeasterlies over the equatorial cold tongue, may play an important role

in enhancing boundary layer winds. For the western/central Pacific, large LHF occurs at the time when the northeast winter monsoon of the western Pacific is strong. In contrast to the aforementioned two regions, LHF in the cold tongue is low and its change is small throughout the year because of low values in dq and SST.

Harmonic analysis is used to quantify the phases and amplitudes of the annual variations of flux across the equatorial Pacific. The annual cycle (*i.e.*, first harmonic) in the northeast and north central/western Pacific accounts for over 60 % of the total variance. The maximum in LHF is seen to migrate westward from the northeast Pacific during boreal summer to the dateline during boreal fall/winter. A time-longitude cross section of the meridionally averaged flux also shows a westward migration of the core region of the LHF. Despite the fact that SST exhibits a strong annual cycle, the semiannual cycle (*i.e.*, second harmonic) of LHF overshadows the annual cycle in the bulk of the cold tongue region. This prominent semiannual cycle is
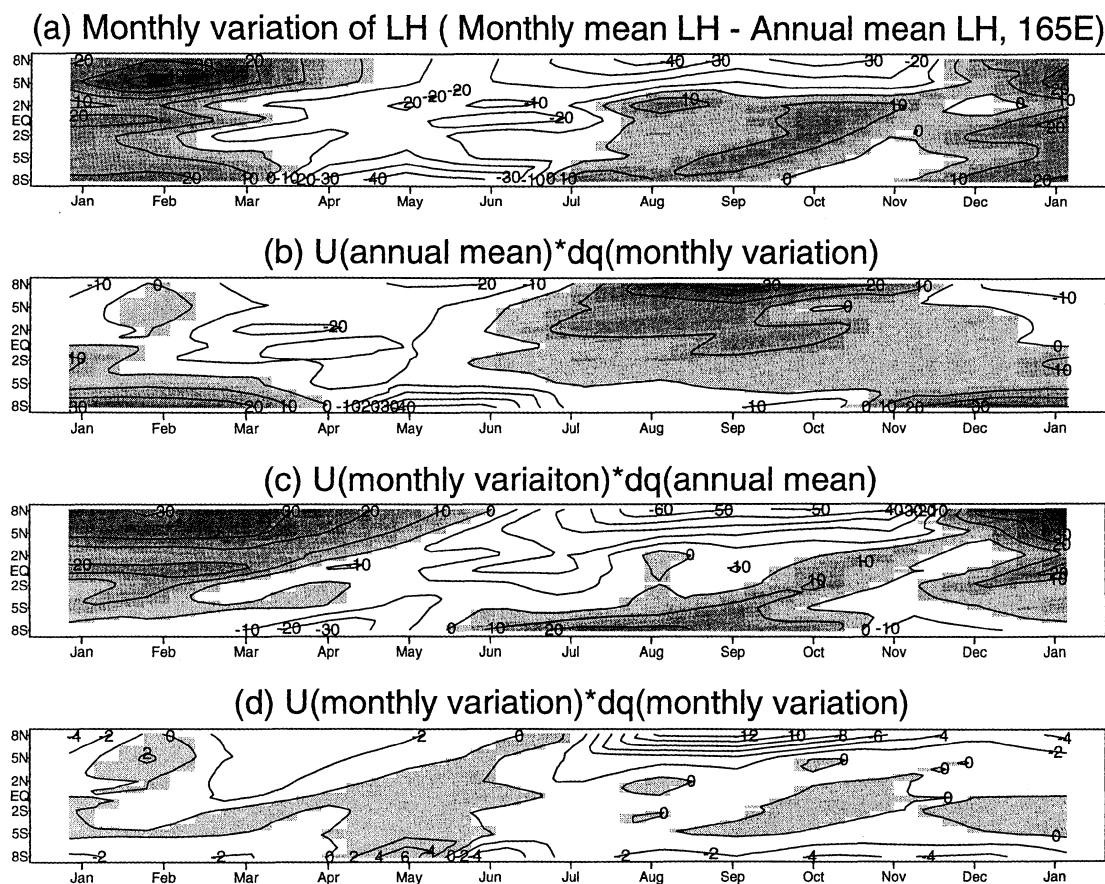
(a) Monthly variation of LH (Monthly mean LH - Annual mean LH, 165E)

(b) U(annual mean)*dq(monthly variation)

(c) U(monthly variaiton)*dq(annual mean)

(d) U(monthly variation)*dq(monthly variation)

Fig. 12. Same as Fig. 10, except for the western Pacific along 165°E.

caused by the weak wind speed in boreal spring and the decrease of dq in boreal fall when SST in the cold tongue reaches its minimum.

The wind speed and humidity difference variables in the bulk aerodynamic formula are partitioned into an annual mean and a deviation quantity. An analysis is made to examine the relative contribution of each term to the monthly variation of LHF along two meridional transects in the equatorial Pacific. It is found that thermodynamic processes are most important for the variation of LHF in the eastern Pacific. However, an exception is a region to the north of the cold tongue during boreal summer in which dynamic processes are equally important as thermodynamic processes to the variation of heat flux. In the western Pacific, monthly variations of LHF induced by wind often dominate those induced by humidity difference, and as a result, dynamic processes are fundamental to the variation of LHF throughout the year. As a final note, the TAO data set can be used for other purposes, such as for calibrating a satellite retrieval algorithm and providing ground truth for surface wind and other air-sea parameters. Moreover, this data set can be used to improve boundary layer parameterizations in ocean-atmosphere models and to validate coupled climate models.

Appendic

Harmonic analysis

Let the k-th ordered harmonic of a given time series of n points ($n = 12$) be represented as

$$X_t = [X] + C_k \cos(2\pi kt/n - \phi_k) \qquad (A1)$$

where X_t is the monthly mean flux series at month ($t = 1, 2, \cdots, 12$), $[X]$ is the grand mean of flux series, ϕ_k the phase angle and C_k denotes the amplitude defined as

$$C_k = (A_k^2 + B_k^2)^{1/2} \qquad (A2)$$

where

$$A_k = \frac{2}{n} \sum_{t=1}^{n} x_t \cos\left(\frac{2\pi kt}{n}\right)$$

$$B_k = \frac{2}{n} \sum_{t=1}^{n} x_t \sin\left(\frac{2\pi kt}{n}\right)$$

The phase angle can be calculated as

$$\phi_k = \begin{cases} \tan^{-1}(B_k/A_k), & A_k > 0 \\ \tan^{-1}(B_k/A_k) \pm \pi, & A_k < 0 \\ 90° \text{ or } 270°. & A_k = 0 \end{cases} \qquad (A3)$$

The portion of variance accounted for by the k-th harmonic is

$$VR_k = \frac{(n/2)C_k^2}{(n-1)S_x^2} \qquad (A4)$$

where S_x^2 is the sample variance of the data series.

References

Bjerknes, J., 1969: Atmospheric teleconnections from the equatorial Pacific. *Mon. Wea. Rev.*, **97**, 526–535.

Chou, S.-H., R.A. Atlas and C.-L. Shie, 1995: Estimates of surface humidity and latent heat fluxes over oceans from SSM/I data. *Mon. Wea. Rev.*, **123**, 2405–2425.

da Silva, A.M., C.C. Young and S. Levitus, 1995: Atlas of surface marine data, Volume 1: Algotithma and procedures. NOAA atlas NESDIS 6, U.S. Department of Commerce.

Deser, C. and J.M. Wallace, 1990: Large-scale atmospheric circulation features of warm and cold episodes in the tropical Pacific. *J. Climate*, **3**, 1254–1281.

Esbensen, S.K. and R.W. Reynolds, 1981: Estimating monthly averaged air-sea transfers of heat and momentum using the bulk aerodynamic method. *J. Phys. Oceanogr.*, **11**, 457–465.

Esbensen, S.K. and Y. Kushnir, 1981: The heat budget of the global ocean: An atlas based on estimates from surface marine observations. Climate Research Institute Rep. No. 29, Oregon State University, Corvallis, OR, 27pp +plates.

Esbensen, S.K. and M.J. McPhaden, 1996: Enhancement of tropical ocean evaporation and sensible heat flux by atmospheric mesoscale systems. *J. Climate*, **9**, 2307–2325.

Fairall, C.W., E.F. Bradley, D.P. Rogers, J.B. Edson and G.S. Young, 1996: Bulk parameterization of air-sea fluxes for Tropical Ocean-Global Atmosphere Coupled-Ocean Atmosphere Response Experiment. *J. Geophys. Res.*, **101**, C2, 3747–3764.

Godfrey, J.S. and A.C.M. Beljaars, 1991: On the turbulent fluxes of buoyancy, heat, and moisture at the air-sea interface at low wind speed. *J. Geophys. Res.*, **96**, 22043–22048.

Horel, J.D., 1982: On the annual cycle of the tropical Pacific atmosphere and ocean. *Mon. Wea. Rev.*, **110**, 1863–1878.

Koberle, C. and S.G.H. Philander, 1994: On the processes that control seasonal variations of sea surface temperatures in the tropical Pacific Ocean. *Tellus*, **46A**, 481–496.

Liu, W.T., 1988: Moisture and latent heat flux variabilities in the tropical Pacific derived from satellite data. *J. Geophys. Res.*, **93**, 6749–6760, plus 6965–6968.

Liu, W.T., K.B. Katsaros and J.A. Businger, 1979: Bulk parameterization of air-sea exchanges of heat and water vapor including the molecular constraints at the interface. *J. Atmos. Sci.*, **36**, 1722–1735.

McPhaden, M.J., 1993: TOGA-TAO and the 1991–93 El Niño Southern Oscillation event. *Oceanogr.*, **6**, 36–44.

Mitchell, T.P. and J.M. Wallace, 1992: On the annual cycle in equatorial convection and sea-surface temperature. *J. Climate*, **5**, 1140–1156.

Myers, G., 1979: Annual variation in the slope of the 14°C isotherm along the equator in the Pacific Ocean. *J. Phys. Oceanogr.*, **9**, 885–891.

Oberhuber, J.M., 1988: An atlas based on the COADS data set: The budgets of heat, buoyancy and turbulent kinetic energy at the surface of the global ocean. Max-Planck Institut fur Meteorologie Rep. No. 15, Hamburg, 20pp +plates.

Reed, R.K., 1985: An estimate of the climatological heat fluxes over the tropical Pacific Ocean. *Clim. and Appl. Met.*, **24**, 833–840.

Sadler, J.C., M.A. Lander, A.M. Hori and L.K. Oda, 1987: Tropical marine climatic atlas. *Vol. 1: Pacific Ocean*. Department of Meteorology, University of Hawaii, 27pp.

Sui, C.-H., X. Li, K.-M. Lau and D. Adamec, 1997: Multiscale air-sea interactions during TOGA COARE. *Mon. Wea. Rev.*, **125**, 448–462.

Trenberth, K.E. and T.J. Hoar, 1996: The 1990–1995 El Niño-Southern Oscillation event: Longest on record. *Geophy. Res. Let.*, **23**, 57–60.

Wallace, J.M., T.P. Mitchell and C. Deser, 1989: The influence of sea surface temperature on surface wind in the eastern equatorial Pacific: Seasonal to interannual variability. *J. Climate*, **2**, 1492–1499.

Wang, B., 1994: On the annual cycle in the tropical eastern central Pacific. *J. Climate*, **7**, 1926–1942.

Weare, B.C., P.T. Strub and M.D. Samuel, 1981: Annual mean surface heat fluxes in the tropical Pacific Ocean. *J. Phys. Oceanogr.*, **11**, 705–717.

Xie, S.-P., 1994: On the genesis of the equatorial annual cycle. *J. Climate*, **7**, 2008–2013.

Zhang, G.J., 1995: Use of monthly mean data to compute surface turbulent fluxes in the tropical Pacific. *J. Climate*, **8**, 3084–3090.

Zhang, G.J. and M.J. McPhaden, 1995: The relationship between sea surface temperature and latent heat flux in equatorial Pacific. *J. Climate*, **8**, 589–605.

Zhang, G.J., V. Ramanathan and M.J. McPhaden, 1995: Convection-evaporation feedback in the equatorial Pacific. *J. Climate*, **8**, 3040–3051.

Zeng, X. and R.E. Dickinson, 1998: Impact of skin temperature on diurnal and monthly surface fluxes over the tropical Pacific. *J. Climate*, in press.

TAO ブイ観測に基づく赤道太平洋上の潜熱フラックスの年周期について

H.-K. Lee・P.-S. Chu
（ハワイ大学気象学教室）
C.-H. Sui・K.-M. Lau
（NASA/ゴダート宇宙飛行センター）

　　熱帯太平洋 (8°N–8°S) の 1992 年から 1996 年までの期間について日平均の TAO ブイ観測データを使用して、海洋上の潜熱フラックス (LHF) と関連するバルク変数 (海面水温、風速、湿度差) の年周期について調べた。西部太平洋で頻繁に観測される活発な対流と弱風を説明するために、改良型バルクパラメタリゼーションスキームを用いて LHF を計算した。また、年周期と半年周期の振幅・位相を同定するために調和解析を適用した。

　　LHF の年周期は二つの地域、北東太平洋と西部/中部太平洋で特徴的な違いがみられた。前者の地域では、海上風速が強く、海面と大気境界層の底面付近との間の温度差が大きい北半球夏季および初秋の時期に LHF の極大が生じていた。西部/中部太平洋では、冬季モンスーンが強い北半球冬季で LHF の極大が生じていた。これらの二つの地域とは対照的に、赤道 cold tongue 域の LHF の年周期は弱く、年を通して LHF は小さい。また、LHF の極大域は 7 月頃北東太平洋にあり、次の年の 3 月までには西部太平洋に達する、西への位相伝播がみられる。

　　LHF の月々の変動を規制している力学的および熱力学的プロセスの相対的な重要性を、東部太平洋と西部太平洋の二つの経度断面で調べてみると、東部太平洋では cold tongue 域の北を除き、湿度差の変動 (熱力学的プロセス) が主として LHF の年変化に重要であると考えられる。一方、西部/中部太平洋の LHF には海上風の風速変動 (力学的プロセス) がより重要である。